Emergent Surface Tension in Vibrated, Noncohesive Granular Media

James P. D. Clewett,[1] Klaus Roeller,[2] R. M. Bowley,[1] Stephan Herminghaus,[2] and Michael R. Swift[1]

[1]*School of Physics and Astronomy, University of Nottingham, Nottingham NG7 2RD, United Kingdom*
[2]*Max Planck Institute for Dynamics and Self-Organization, Am Faßberg 17, 37077 Göttingen, Germany*
(Received 9 July 2012; published 30 November 2012)

We describe experiments and simulations carried out to investigate spinodal decomposition in a vibrated, dry granular system. The dynamics is found to be similar to that of systems evolving under curvature-driven diffusion, which suggests the presence of an effective surface tension. By studying quasi-2D droplets in the steady state, we find behavior consistent with Laplace's equation, demonstrating the existence of an actual surface tension. Detailed measurements of the pressure tensor in the interfacial region show that the surface tension results predominantly from an anisotropy in the kinetic energy part of the pressure tensor, in contrast to thermodynamic systems where it arises from either the attractive interaction between particles or entropic considerations.

Despite many decades of dedicated research, the basic principles governing the physics of many-body systems far from equilibrium are still elusive [1]. In particular, such systems can exhibit emergent collective behavior, which on the basis of current knowledge cannot be predicted from the properties of their microscopic components [2,3]. A particularly simple environment for investigating nonequilibrium physics is that of granular media [4,5]. There are numerous examples of pattern formation in granular systems driven far from equilibrium [6–9], where order frequently results from the appearance of distinct phases separated by an interface. For systems in thermodynamic equilibrium, interfaces generally are associated with an excess free energy per unit area, referred to as the surface tension. Microscopically, surface tension may arise from attractive intermolecular forces [10] and entropic contributions [11]. However, in a dry granular media, there are neither appreciable attractive nor a well-defined entropy.

Phase separation has been predicted [12–14] and observed [15] in quasi-1D-driven granular systems and quasi-2D vibrated, granular monolayers [16]. Recently, it has been shown that a loosely confined, vertically vibrated, dry granular gas exhibits a quasi-2D phase separation into a dense liquidlike phase and a dilute gaslike phase [17], closely reminiscent of phase separation in a regular liquid. The phase separation was shown to be linked to a negative compressibility in the homogeneous system, and a spinodal was found that arises from an excess in the kinetic energy of the dilute phase due to resonant motion of the particles.

It is of great conceptional interest whether a surface tension can be consistently assigned to the phase boundary in this system. The existence of a surface tension may pave the way to establishing a quantity analogous to the free energy for many-body systems far from thermal equilibrium. In this Letter, we describe experiments and simulations carried out to investigate the coarsening dynamics and interfacial properties of a vibrated, dry granular

system. The phase separation is spinodal driven, and the dynamics of the decomposition is found to be compatible with a standard scenario with conserved order parameter [18]. By studying quasi-2D droplets in simulations, we find behavior consistent with Laplace's equation, demonstrating the existence of a surface tension. The surface tension can also be derived from pressure tensor measurements in the interfacial region. Simulations allow us to independently measure the contributions from the kinetic and collisional parts of the pressure tensor. Our findings show that the surface tension predominantly results from an anisotropy in the kinetic part of the pressure tensor.

Our experimental apparatus consists of a glass cell that can be vibrated vertically using an electromagnetic shaker. The cell was constructed using a square glass base, on top of which we attached a square frame of height $h = 3$ mm, creating a square horizontal tray of edge length $L = 180$ mm. Bronze spheres, with diameter d in the range $150 \ \mu m < d < 180 \ \mu m$, were placed in the tray and enclosed with a top plate identical to the base. We define the mean volume filling fraction $\bar{\phi}$ as the total volume of the particles divided by the interior volume of the cell. The upper and lower glass plates were 6 mm thick to provide necessary rigidity. Prior to each measurement the glass plates were cleaned and wiped with an antistatic coating to reduce charging effects. The cell was clamped to the electromagnetic shaker and vibrated sinusoidally at a fixed frequency, f, and amplitude, A, giving a maximum dimensionless acceleration relative to gravity, g, of $\Gamma = A(2\pi f)^2/g$. Care was taken to ensure that the cell was level and that the structure did not flex under vibration. The apparatus was observed from above using a digital camera with resolution 640×480 pixels with a frame rate of 30 fps.

Simulations were carried out with parameters matching the experiment as closely as possible with available computing power. We used soft-sphere molecular dynamic simulations of identical spherical particles, diameter
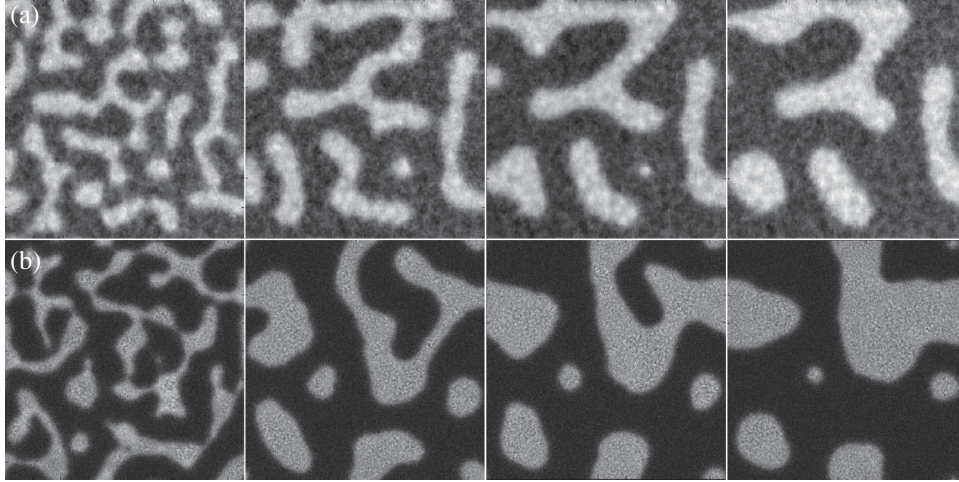
FIG. 1.   Snapshots of granular spinodal decomposition taken from (a) experiment, and (b) simulation (see Supplemental Material [33]). From left to right, the images show the pattern for $ft = 60, 160, 260,$ and 360. The cell is subjected to vertical vibration at $\Gamma \approx 7.2$ and $f = 60$ Hz, corresponding to $A/d = 3.0$. The volume filling fraction is $\bar{\phi} = 0.05$.

$d = 165$ μm and density $\rho = 8900$ kg m^{-3}. Collisions were modeled using linear springs and dash-pot damping, giving rise to a constant coefficient of restitution. Rotation, friction, and the effects of air were neglected. Particles were contained in a volume which matched the dimensions of the experimental cell ($1080d \times 1080d \times 18.2d$). The simulated cell was then subjected to sinusoidal vertical vibration. Periodic boundary conditions in the horizontal directions were used to remove the influence of the cell walls. Simulations to measure the phase diagram and the interfacial profile were carried out in a cell with reduced dimensions of $210d \times 40d \times 18.2d$. To match the experimental phase diagram, we chose a coefficient of restitution $\varepsilon_{pp} = 0.7$ for particle-particle collisions [19] and $\varepsilon_{pg} = 0.8$ for particle-glass collisions. Typical simulations involved up to 2 million particles and were averaged over simulated times up to 18 s. The simulations were carried out using compute unified device architecture on a Tesla Fermi C2050 GPGPU [20].

Figure 1 shows typical sequences of snapshots taken from experiment (a) and simulation (b). The driving parameters were chosen to match the experiment. The system was prepared with the particles homogeneously distributed in the horizontal plane. The mean volume filling fraction of the particles is $\bar{\phi} = 0.05$. Sinusoidal vertical vibration is then suddenly applied, such that a spinodal-driven phase separation occurs. The dense (light) and dilute (dark) regions form locally, and the pattern evolves until it is dominated by a single domain of each phase. Varying A and $\bar{\phi}$ changes the size of the domains in the steady state. The vibration amplitude was selected so that at late times approximately equal amounts of the two phases remain, thus allowing for the longest possible time evolution. Inspection of Fig. 1 suggests that the experiment and simulation evolve in a similar way, implying that the simulation captures the

essence of the coarsening dynamics. Further confirmation that the simulation matches the experiment is presented in Fig. 2(a), where we show the phase diagram for the experiment and for the simulation.

In order to quantify the time evolution of the patterns, the structure factor, $S(\mathbf{k}, t)$, is calculated using the local density data from the simulations and gray scale intensity from the images taken of the experiment. We extract a characteristic length scale for the system, $l(t)$, obtained from $l(t) = 2\pi \sum S(\mathbf{k}, t) / \sum |\mathbf{k}| S(\mathbf{k}, t)$ where the sums are over values of $|\mathbf{k}|$ which satisfy the condition $k > 4\pi/L$ to minimize finite size effects. Figure 2(b) shows the time evolution of $l(t)$. The solid circles (black) show the results from simulations averaged over 10 runs; the crosses (red) show the experimentally measured $l(t)$ also averaged over 10 runs. Time is expressed in terms of the dimensionless quantity ft, where $ft = 0$ is the time at which the vibration is switched on. At $ft \approx 10$, a pattern is visible. Thereafter, the pattern is observed to coarsen with larger domains engulfing smaller ones and small droplets evaporating. At late times, $ft \approx 400$, the slope rolls off due to the finite size of the system. Between these two limits, the length scale $l(t)$ grows approximately as a power law of t, with $l(t) \sim t^{1/3}$, as indicated by the dot-dashed line (green). Figure 2(d) shows the scaling collapse for circularly averaged $S(k, t)$ in the late time regime. Good collapse is obtained for both simulation and experiment if one assumes that the length scale grows as $t^{1/3}$.

The scaling behavior shown in Figs. 2(b) and 2(d) is reminiscent of Cahn-Hilliard theory (often referred to as model B), which describes a system with a conserved order parameter in which the dynamics are diffusive and curvature driven [18]. To test the validity of such a continuum model for our system, we have fitted the form of the steady-state interfacial profile to a function of the form
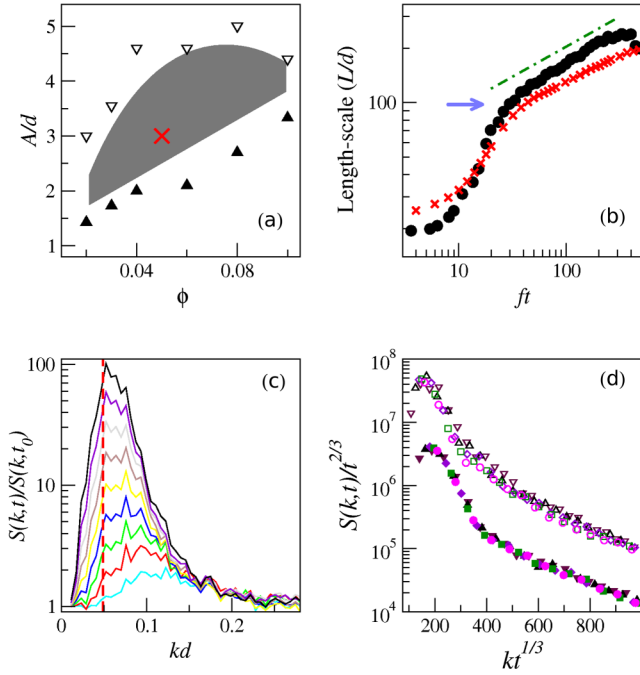
FIG. 2 (color online). (a) Phase diagram obtained from experiment (triangles) and simulation (shaded area). The enclosed region shows the parameters for which spontaneous phase separation occurs (the spinodal region). The conditions for the quench ($A/d = 3.0$, $\bar{\phi} = 0.05$) are marked by the cross (red); (b) time evolution of the characteristic length scale, $l(t)$, during spinodal decomposition obtained from experiment (red crosses) and simulation (solid black circles). The dot-dashed line (green) has a slope of 1/3 as a guide to the eye; (c) early time evolution of $S(k, t)$ obtained from simulations for ft linearly spaced in the range $4 \leq ft \leq 20$, with the topmost curve being $ft = 20$ and $ft_0 = 2$. The vertical red dashed line indicates the fastest growing wave number predicted by assuming model B dynamics, k_c; (d) collapse of $S(k, t)$ in the scaling regime, assuming a growth law of $t^{1/3}$. The experimental (solid) data points have been shifted vertically relative to the simulation (hollow) for clarity.

$\phi(z) = \phi_g + \frac{1}{2}(\phi_l - \phi_g)[1 - \tanh(z/\xi)]$, which implies a quartic form for the bulk potential [14,15,21,22]. Here, ϕ_l and ϕ_g are the local filling fractions in the dense and dilute phases, respectively, and z is the coordinate normal to the interface. If model B dynamics are appropriate, the steady-state interfacial width predicts the dominant length scale after the early time exponential growth, with corresponding wave number $k_c = 1/\xi$ [23,24]. The predicted wave number is shown in Fig. 2(c) by the vertical red dashed line, and the corresponding length scale is shown by the arrow in Fig. 2(b), demonstrating consistency with model B.

To further corroborate these findings, a deeper investigation of surface tension effects is in order. Given the qualitative and quantitative agreement between the simulation and the experiment, both in the steady state and in the coarsening dynamics, the simulation captures the
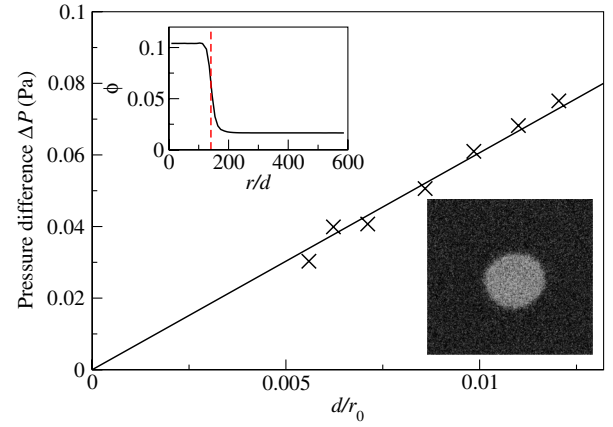
FIG. 3 (color online). The main panel shows the difference in horizontal pressure, ΔP, between the inside and the outside of a circular droplet as a function of the inverse of the droplet radius, r_0. The lower inset shows an image from simulation where the final configuration is a circular droplet ($\bar{\phi} = 0.025$). The upper inset shows the mean local filling fraction, ϕ, of the droplet as a function of the radial coordinate r. The dashed line (red) marks the position of r_0 at the mean filling fraction of the two phases. The width of the interface shown is independent of $\bar{\phi}$ for large droplets.

essential physics of this system even though the simulations ignore friction, particle rotation, and the possible influence of air. We will henceforth focus on data from simulations that allow us to measure quantities such as the local density and the local pressure tensor that are not readily obtainable from our experiment. For consistency with the experimental data, simulated quantities are expressed in SI units where appropriate.

One of the signatures of a surface tension is that the system evolves to minimize the interfacial area. In quasi-2D with periodic boundary conditions, the two possible geometric configurations that do this are a single stripe or a circular droplet. Examples of droplets can be seen in Fig. 1. If the simulations presented in Fig. 1 are allowed to continue until a steady state is reached, a single circular dense droplet remains, provided that the filling fraction is small enough, $\bar{\phi} \lesssim 0.04$. An example of such a droplet is shown in the lower inset of Fig. 3. The circularly averaged local density is shown in the upper inset, from which we determine the radius of the droplet, r_0.

If there is an effective surface tension holding the circular droplet together, then from Laplace's law, there must be a pressure difference, ΔP, between the two phases. We measure ΔP in simulation using the mean local horizontal pressure in the dense and dilute phases. The local pressure is obtained from the virial theorem [25] in terms of the kinetic and collisional parts. We confirm that for our droplets the pressure is uniformly higher inside than outside. The main panel of Fig. 3 shows ΔP as a function of $1/r_0$ for $85d < r_0 < 182d$. For mechanical stability,
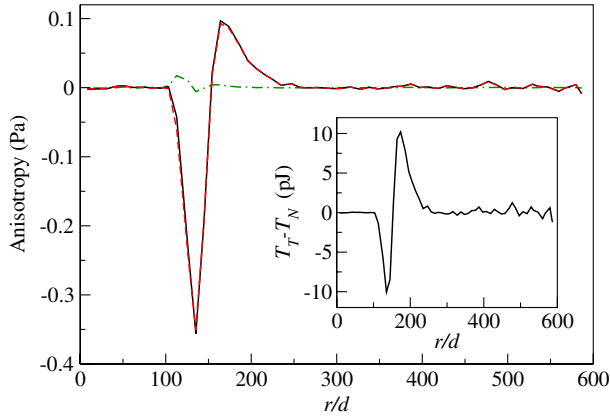
FIG. 4 (color online). The main panel shows the difference in the normal and tangential components of (a) the total pressure tensor (black line), (b) the kinetic part of the pressure tensor (red line), and (c) the collisional part of the pressure tensor (dot-dashed green line). The difference in the normal and tangential components of the total pressure tensor closely follows the anisotropy in the kinetic part of the pressure tensor. The inset shows the difference between the normal and tangential components of the kinetic energy per particle (Supplemental Material [33]).

Laplace's equation in 2D relates ΔP to the surface tension, σ, by the equation $\Delta P = \sigma/r_0$. Due to the small height of the cell, there is no phase separation or curvature in the vertical direction. The measured horizontal pressure difference is consistent with a curvature-independent surface tension $\sigma = 1.0 \pm 0.1 \times 10^{-3}$ N m^{-1}. (In comparison the surface tension of water at STP is 7×10^{-2} N m^{-1}.)

Alternatively, one may use a mechanical definition of surface tension to calculate σ in terms of the normal and tangential components of the pressure tensor. For a circular droplet, σ is given by

$$\sigma = r_0 \int_0^\infty \frac{1}{r}[p_N(r) - p_T(r)]dr, \qquad (1)$$

where $p_N(r)$ is the component of the pressure tensor normal to the interface, $p_T(r)$ is the component of the pressure tensor tangential to the interface, and r is the radial distance from the center of the droplet [10,26].

The main panel of Fig. 4 shows the circular average of the pressure anisotropy $p_T - p_N$ as a function of radial position for a droplet of radius $140d$ (solid black line). The pressure difference exhibits a dip in the interfacial region which, via Eq. (1), is the source of the surface tension. Evaluating the integral for various droplet sizes gives a mean surface tension of $\bar{\sigma} = 0.94 \pm 0.05 \times 10^{-3}$ N m^{-1}, in very good agreement with the value obtained above from Laplace's equation. This demonstrates an unexpectedly high degree of analogy between the phase-separating granular system and an equilibrium thermodynamic

system, concerning the existence of a surface tension as well as the role of the latter in the coarsening dynamics. Although coarsening has been observed in other granular systems [15,27–29], the corresponding dynamics has so far not been conclusively interpreted [8].

In order to understand the microscopic origin of the surface tension in our system, we consider the kinetic and collisional parts of the pressure tensor separately. The anisotropy in the kinetic energy part of the pressure tensor is shown by the red line (dashed) in Fig. 4; the corresponding anisotropy in the collisional part of the pressure tensor is shown by the green line (dot-dashed). Since the anisotropy in the kinetic part of the pressure tensor closely follows the anisotropy in the total pressure tensor, it is clear that the dominant contribution to the surface tension arises from the anisotropy in the kinetic energy tensor alone; the anisotropy in the collisional part of the pressure tensor is negligible.

Finally, we may inquire about the cause of this anisotropy in our far-from-equilibrium system. The inset to Fig. 4 shows the difference between the normal, T_N, and tangential, T_T, components of the kinetic energy *per particle*. Close to the interface in the dilute region, there is a slight excess in T_T relative to T_N. In the dense region, T_T is somewhat reduced relative to T_N. To explain this variation we consider a simple mechanistic picture of a single particle incident on the interface from the dilute phase. On average, the component of the kinetic energy normal to the interface is reduced due to inelastic collisions with the dense phase; in contrast, the tangential component is largely unaffected. Therefore, T_N in the dilute phase is reduced relative to T_T, as observed. The normal component of momentum is transferred into the dense phase, leading to a slight excess in the local T_N just inside the surface of the droplet. When T_N and T_T are weighted by the local density (upper inset in Fig. 3), the resulting kinetic part of the pressure tensor in the dense region is strongly enhanced relative to the dilute region. This gives rise to the asymmetry about the interface shown in the main panel of Fig. 4.

Anisotropies in kinetic energy are known to occur in driven granular gases [30–32]. In these systems, the anisotropy is strongly coupled to the driving mechanism. In contrast, the anisotropy in our system arises from a spontaneous symmetry breaking in the horizontal components of the kinetic energy caused by the dissipative interaction at the interface.

Our results demonstrate the existence of a minimization principle in a phase-separated granular gas, implying an effective far-from-equilibrium free energy. The coarsening dynamics are consistent with the steady-state measurements of an emergent surface tension. The simple mechanistic explanation of a kinetic energy tensor anisotropy provides an understanding of this surface tension in a noncohesive dissipative gas. The general nature of the

argument suggests that it may well be applicable to other granular phenomena in which interfaces exist between phases [8,9,15,16] and that anisotropy in the kinetic energy tensor is a possible driving mechanism for emergent collective behavior in many nonequilibrium systems.

[1] H. Jaeger and A. J. Liu, arXiv:1009.4874v1.

[2] J. M. Carlson and J. Doyle, Proc. Natl. Acad. Sci. U.S.A. **99,** 2538 (2002).

[3] J. H. P. Dawes, Phil. Trans. R. Soc. A **368,** 3519 (2010).

[4] H. M. Jaeger, S. R. Nagel, and R. P. Behringer, Rev. Mod. Phys. **68,** 1259 (1996).

[5] H. J. Herrmann and S. Luding, Continuum Mech. Thermodyn. **10,** 189 (1998).

[6] P. B. Umbanhowar, F. Melo, and H. L. Swinney, Nature (London) **382,** 793 (1996).

[7] F. Melo, P. Umbanhowar, and H. L. Swinney, Phys. Rev. Lett. **72,** 172 (1994).

[8] I. S. Aranson and L. S. Tsimring, Rev. Mod. Phys. **78,** 641 (2006).

[9] A. Prevost, P. Melby, D. A. Egolf, and J. S. Urbach, Phys. Rev. E **70,** 050301 (2004).

[10] J. S. Rowlinson and B. Widom, *Molecular Theory of Capillarity* (Oxford University Press, New York, 1982).

[11] W. G. Hoover and F. H. Ree, J. Chem. Phys. **49,** 3609 (1968).

[12] E. Livne, B. Meerson, and P. V. Sasorov, Phys. Rev. E **65,** 021302 (2002).

[13] J. J. Brey, M. J. Ruiz-Montero, F. Moreno, and R. García-Rojo, Phys. Rev. E **65,** 061302 (2002).

[14] M. Argentina, M. G. Clerc, and R. Soto, Phys. Rev. Lett. **89,** 044301 (2002).

[15] M. G. Clerc, P. Cordero, J. Dunstan, K. Huff, N. Mujica, D. Risso, and G. Varas, Nat. Phys. **4,** 249 (2008).

[16] A. E. Lobkovsky, F. Vega Reyes, and J. S. Urbach, Eur. Phys. J. Special Topics **179,** 113 (2009).

[17] K. Roeller, J. P. D. Clewett, R. M. Bowley, S. Herminghaus, and M. R. Swift, Phys. Rev. Lett. **107,** 048002 (2011).

[18] A. J. Bray, Adv. Phys. **43,** 357 (1994).

[19] C. Bizon, M. D. Shattuck, J. B. Swift, W. D. McCormick, and H. L. Swinney, Phys. Rev. Lett. **80,** 57 (1998).

[20] J. A. Anderson, C. D. Lorenz, and A. Travesset, J. Comput. Phys. **227,** 5342 (2008).

[21] J. W. Cahn and J. W. Hilliard, J. Chem. Phys. **28,** 258 (1958).

[22] C. Cartes, M. G. Clerc, and R. Soto, Phys. Rev. E **70,** 031302 (2004).

[23] J. W. Cahn, J. Chem. Phys. **42,** 93 (1965).

[24] K. R. Elder, T. M. Rogers, and R. C. Desai, Phys. Rev. B **38,** 4725 (1988).

[25] H. Goldstein, *Classical Mechanics* (Addison-Wesley, Reading, MA, 1950).

[26] M. J. Nijmeijer, C. Bruin, A. B. van Woerkom, A. F. Bakker, and J. M. J. van Leeuwen, J. Chem. Phys. **96,** 565 (1992).

[27] I. S. Aranson, B. Meerson, P. V. Sasorov, and V. M. Vinokur, Phys. Rev. Lett. **88,** 204301 (2002).

[28] M. V. Sapozhnikov, Y. V. Tolmachev, I. S. Aranson, and W.-K. Kwok., Phys. Rev. Lett. **90,** 114301 (2003).

[29] T. Y. Wang and T. M. Hong, Phys. Rev. E **78,** 061301 (2008).

[30] D. van der Meer and P. Reimann, Europhys. Lett. **74,** 384 (2006).

[31] D. J. Holland, C. R. Müller, J. S. Dennis, L. F. Gladden, and A. J. Sederman, Powder Technol. **182,** 171 (2008).

[32] S. Luding, Nonlinearity **22,** R101 (2009).

[33] See Supplemental Material at http://link.aps.org/supplemental/10.1103/PhysRevLett.109.228002 for movies showing the time evolution of the spinodal decomposition and an image showing the kinetic energy anisotropy around a circular droplet.